ACS APPLIED MATERIALS & INTERFACES

Article

Effective and Selective Trapping of Volatile Organic Sulfur Derivatives by Montmorillonite Intercalated with a μ-oxo Fe(III)-Phenanthroline Complex

Fabrizio Bernini, Elena Castellini, Daniele Malferrari, Germán Rafael Castro, Claro Ignacio Sainz-Diaz, Maria Franca Brigatti, and Marco Borsari

ACS Appl. Mater. Interfaces, **Just Accepted Manuscript** • DOI: 10.1021/acsami.6b11906 • Publication Date (Web): 12 Dec 2016

ACS Publications

ACS Applied Materials & Interfaces is published by the American Chemical Society. 1155 Sixteenth Street N.W., Washington, DC 20036

Effective and Selective Trapping of Volatile Organic Sulfur Derivatives by Montmorillonite Intercalated with a μ-oxo Fe(III)-Phenanthroline Complex

Fabrizio Bernini,[a] Elena Castellini,*[a] Daniele Malferrari,[a] German Rafael Castro,[bc] Claro Ignacio Sainz Díaz,[d] Maria Franca Brigatti[a] and Marco Borsari[a].

* Corresponding author (E-mail: elena.castellini@unimore.it)

[a] Department of Chemical and Geological Sciences, University of Modena and Reggio Emilia, Via Campi 103, I-41125 Modena, Italy

[b] SpLine, Spanish CRG BM25 Beamline at the ESRF, 6 Jules Horowitz, F-38043 Grenoble, France

[c] Instituto de Ciencia de Materiales de Madrid (ICMM), CSIC, c. Sor Juan Inés de la Cruz 3, E-28049 Madrid, Spain.

[d] Instituto Andaluz de Ciencias de la Tierra (IACT) CSIC, Universidad de Granada, Av.da Las Palmeras 4, 18100 Granada, Spain.

ABSTRACT

The μ-oxo Fe(III)-phenanthroline complex $[(OH_2)_3(Phen)FeOFe(Phen)(OH_2)_3]^{+4}$ intercalated in montmorillonite provides a stable hybrid material. In this study, the ability and efficiency of this material to immobilize thiols in gas phase, acting as a trap at the solid-gas interface, were investigated. Aliphatic thiols containing both hydrophilic and hydrophobic end groups were chosen to test the selectivity of this gas trap. DR-UV-Vis, IR, elemental analysis, thermal analysis and evolved gas mass spectrometry, X-ray powder diffraction, and X-ray absorption spectroscopy techniques were employed to characterize the hybrid material before and after thiol exposure and to provide information on the entrapping process. Thiol immobilization is very large, up to 21% w/w for heptanethiol. In addition, evidence was obtained that immobilization occurs through the formation of a covalent bond between the iron of the complex and the sulfur of the thiol. This provides an immobilization process characterized by a higher stability with respect to the methods based on physi-adsorption. Thiol immobilization resulted thermally reversible at least for 20 adsorption/desorption cycles. Unlike standard desulfurization processes like hydrotreating and catalytic oxidation which work at high temperatures and pressures, the present system is able to efficiently trap thiols at room temperature and pressure, thus saving energy. Furthermore, we found that the selectivity of thiol immobilization can be tuned acting on the amount of complex intercalated in montmorillonite. In particular, montmorillonite semi-saturated with the complex captures both hydrophobic and hydrophilic thiols, while the saturated montmorillonite shows a strong selectivity towards the hydrophobic molecules.

KEY WORDS

Iron-phenanthroline complex, montmorillonite, heptanethiol, solid-gas interface, sulfur trapping, thiol, mercaptohexanol.

INTRODUCTION

Volatile sulfur compounds, such as thiols, are common air pollutants found in several anthropic backgrounds like petrochemical and gasification plants, wastewater treatment plants, and solid waste landfills. These smelly gas emissions, when released in a great amount in the atmosphere may behave as greenhouse gases and could therefore be a possible source of acidic rains. As natural hydrocarbons like natural gas and petroleum contain large levels of thiols and H_2S,[1,2] their use as fuel sources should be severely controlled. Their burning in fact releases SO_2 and other toxic volatile sulfur-containing compounds in the atmosphere. One of the key actions needed to make the environmental protection compatible with the growing global energy demand is therefore to develop materials and processes that get rid of the sulfur-containing compounds from disposable fuel sources with high efficiency.[3] Moreover, desulfurization is a mandatory step in oil refining processes, as sulfur poisons the catalyst employed in the reforming step for octane production. In addition, it is known that a high sulfur content strongly lowers the quality of automotive gasoline.

In the last two decades, a number of adsorption materials and catalyzers based on surface modified clays were prepared.[4-10] Most of the efforts were directed to the understanding of the interaction with carbon dioxide, hydrocarbons (methane in particular), and hydrogen sulfide.[11-20] In fact, some distinctive properties such as microporosity, wettability and a negative surface charge, make several naturally occurring clay minerals suitable materials for gas sequestration and selective trapping. Carbon dioxide, essentially by virtue of its quadrupole moment, can be intercalated inside the interlayer of smectites. Methane has no quadrupole moment, but can interact with clay minerals because of its large polarizability as well as hydrogen sulfide. The latter has much more affinity for the hydrophilic montmorillonite framework than carbon dioxide and methane. Furthermore, the capacity of hydrated layer silicates such as montmorillonite to store carbon dioxide, methane and hydrogen sulfide strongly depends on the presence of pre-adsorbed water, which cannot be avoided owing to the hydrophilic nature of this clay.[16,21] However, irreversibly dehydrated and modified clays can be used as well. In fact, a successful tool for hydrogen sulfide removal from wet air streams can be found in metal-doped pillared clays, thanks to the homogenous micropore structure and the high dispersion in the layer of the catalytically active metal. [11,19,20]

Although an abundant literature is available on the interaction between natural or modified clay minerals and carbon dioxide, methane, and hydrogen sulfide at the solid-gas interface, little is known about the interaction between layered minerals and thiols.[22-25] Hydrophobicity of thiols that lowers the affinity for the hydrophilic clay minerals may have inhibited research in this area. Of course, direct adsorption of thiols on the surface of natural clay minerals is not possible. However,

adsorption can be obtained if the hydrophilic surface is transformed into a hydrophobic medium. Importantly, the swelling behavior of clay that allows large molecules to be hosted in the interlayer must be preserved. Therefore, any treatment that would result in a deep structural modification of the layer must be avoided. Following this approach, here we show how new hybrid materials made by montmorillonite (Mt) intercalated with the μ-oxo Fe(III)-phenanthroline complex $[(OH_2)_3(Phen)FeOFe(Phen)(OH_2)_3]^{+4}$ (Fe(III)Phen),[26] are able to efficiently trap volatile sulfur compounds at the solid-gas interface at room temperature and pressure. These new materials (Mt-Fe(III)Phen) were extensively investigated in a previous paper.[26] In particular, two types of Mt-Fe(III)Phen, structurally different, were obtained. The semi-saturated material (Mt-Fe(III)$Phen_{semi-sat}$) was prepared intercalating an amount of complex corresponding to the CEC of Mt. The saturated material (Mt-Fe(III)$Phen_{sat}$), instead, was obtained intercalating Mt with an amount of Fe(III) complex twice the CEC value. In this case, sulfate ions were found to be co-adsorbed inside the interlayer to compensate the positive charge in excess with respect to the CEC. The properties of the Mt-Fe(III)Phen hybrid materials resulted to be strongly affected by the amount of the intercalated complex, in particular a noticeable restructuration of the interlayer is observed with saturation.[26] As such, the process of gas immobilization exploits a natural, cheap, easily available entrapping material and does not need any energy supply. The Mt-Fe(III)Phen hybrid materials employed, are able to immobilize hydrophobic thiols and, only under specific conditions, hydrophilic thiols. Binding does not occur *via* van der Waals interactions, but through a redox reaction and a binding process that involve the gas phase and the iron complex. Chemisorption of thiols from gas phase mixtures was previously obtained only using gold nanoparticles supported on metal oxides.[27] This hybrid material efficiently removes thiols from gaseous phases with a procedure which may be easily extended to liquid phase hydrocarbons and even directly applicable to liquid hydrocarbons, oil, gasoline and diesel.

The trapping material is able to immobilize thiols through covalent bonds to the iron center, providing a more efficient and stronger retention than those relying on physiadsorption.[28,29] Maximum thiols adsorption capacity of this material was determined along with chemical speciation of the absorbent and adsorbate after interaction. The hybrid material shows a high selectivity toward hydrophobic thiols. We also demonstrated the reversibility of the reaction highlighting that the adsorbent can be quickly regenerated also in mild conditions and reused several times before exhaustion. Therefore, promising applicative potentialities can be foreseen, ranging from industrial (e.g., filter, sampling of gases in the workplace, etc.) to large-scale environmental applications.

EXPERIMENTAL SECTION

2.1. Materials

Montmorillonite STx-1a (Mt) was provided by the Clay Minerals Society (The Clay Minerals Society, Source Clays Repository, University of Missouri, Columbia, MO).[30,31] Its CEC is 0.844 equivalents/kg.[30]

All chemicals were of analytical grade (purity > 99%), and purchased from Carlo Erba (acetic acid, $Fe_2(SO_4)_3 \cdot 8H_2O$, and NaOH pellets) and from Sigma Aldrich (1,10-phenanthroline ($C_{12}H_8N_2$, Phen), ferroin ($[Fe^{II}(C_{12}H_8N_2)_3]SO_4$, Fe(II)Phen$_3SO_4$), heptanethiol (SC7), undecanethiol (SC11), 6-mercapto-1-hexanol (SC6OH), 11-mercapto-1-undecanol (SC11OH), 6-mercaptohexanoic acid (SC5COOH) and 11-mercaptoundecanoic acid (SC10COOH)).

The solutions of the μ-oxo Fe(III)-phenanthroline complex $[(OH_2)_3(Phen)FeOFe(Phen)(OH_2)_3]^{+4}$ (Fe(III)Phen, hereafter) were prepared as reported elsewhere.[26] Their stability as a function of time was checked spectrophotometrically in the pH range 2.5-5.0 (see S1).

2.2. Preparation of montmorillonite saturated and semi-saturated with the μ-oxo Fe(III)-phenanthroline complex

Montmorillonite saturated with Fe(III)Phen (Mt-Fe(III)Phen$_{sat}$ hereafter): solutions of Fe(III)Phen were prepared in 10mM acetate buffer at pH 5.1 dissolving $Fe_2(SO_4)_3 \cdot 8H_2O$ in 6 mM Phen solutions in 1:1 Fe(III)/Phen molar ratio.[26] Batches of suspensions were prepared mixing 20 mg of Mt with 4 mL of 3 mM Fe(III)Phen solutions; the concentration of the freshly prepared Fe(III)Phen solutions was checked spectrophotometrically following the O^{2-}(bridge) → Fe(III) charge-transfer band at 356 nm.[26] The batches were shaken at 250 rpm in an orbital incubator (Stuard Scientific Orbital Incubator SI50) at 20°C for 30 min using a Haake k20 Thermocryostat. Measurements performed at different adsorption times demonstrated that the adsorption process requires less than 30 min to reach the equilibrium. Then, solid-liquid separation was obtained by centrifugation at 14000 rpm (Thermo mod. Espresso Centrifuge) for 1 min. UV-Vis spectra were acquired on the clarified supernatants using a Jasco V-570 spectrophotometer to determine the amount of Fe(III)Phen adsorbed on Mt (typically 0.438±0.014 mol/Kg, *i.e.* 1.752±0.056 eq/Kg). This datum is in complete agreement with that provided by the adsorption isotherm of Fe(III)Phen on Mt and corresponds to the twice of the CEC.[26] These conditions allow considering Mt saturated in Fe(III)Phen.[26] The separated solid, washed several times with distilled water and dried at 30°C, constitutes the Mt-Fe(III)Phen$_{sat}$ material. The liquid after washing was separated each time by

centrifugation and submitted to ICP analysis (ICP Plasma Varian Mod. Liberty 200) to verify the absence of Fe(III)Phen.

Montmorillonite semi-saturated with Fe(III)Phen (Mt-Fe(III)Phen$_{semi-sat}$ hereafter): a similar procedure was used for the preparation of Mt-Fe(III)Phen$_{semi-sat}$. In this case, the batches of suspensions were prepared mixing 20 mg of Mt with 4 mL of 1 mM Fe(III)Phen solutions in 10 mM acetate buffer at pH = 5.1, following the same procedure previously described for the saturated sample. As above, UV-Vis spectra were used to determine the amount of Fe(III)Phen adsorbed on Mt, typically 0.222±0.012 mol/Kg (0.888±0.048 eq/Kg). This datum corresponds to the CEC of Mt. Hereafter, the term Mt-Fe(III)Phen indicates a Mt sample intercalated with the Fe(III)Phen complex regardless of its concentration.

Stability of the intercalated Fe(III)Phen complex and reversibility of the adsorption process were verified through exchange experiments. Mt-Fe(III)Phen$_{sat}$ and Mt-Fe(III)Phen$_{semi-sat}$ were treated with 5M $CaCl_2$ solutions to observe the exchange of Ca^{2+} with the immobilized complex (for details see S2). UV-Vis spectra performed on the exchanged solutions after 30 min fully match those of the pristine complex, in particular the O^{2-}(bridge) → Fe(III) charge-transfer band at 356 nm remains unchanged (see S2, Figures S2a and S2b). Successive exchanges show again the release of the intact complex. The results confirm that the complex is stable inside the interlayer and the intercalation for both Mt-Fe(III)Phen$_{sat}$ and Mt-Fe(III)Phen$_{semi-sat}$ is reversible.

Montmorillonite treated with $[Fe(II)Phen_3]^{2+}$ (Mt-Fe(II)Phen$_3$ hereafter): a 3 mM solution of $[Fe(II)Phen_3]^{2+}$ (Fe(II)Phen$_3$, hereafter) was prepared dissolving a proper amount of $Fe(II)Phen_3SO_4$. Analogously to Fe(III)Phen, a suspension was prepared mixing 20 mg of Mt with 4 mL of the 3 mM Fe(II)Phen$_3$ solution, it was shaken at 250 rpm in an orbital incubator (Stuard Scientific Orbital Incubator SI50) at 20°C (Haake k20 Thermocryostat) for 30 min. The solid phase was separated by centrifugation at 14000 rpm (Thermo mod. Espresso Centrifuge) for 1 min, washed several times with distilled water and dried at 30°C (Mt-Fe(II)Phen$_3$).

2.3. Immobilization of thiols on Mt-Fe(III)Phen$_{sat}$ and Mt-Fe(III)Phen$_{semi-sat}$

The immobilization of thiols on Mt and Mt-Fe(III)Phen was performed at 20°C in a closed glass box covered with an aluminum foil. 100 mg of Mt-Fe(III)Phen$_{sat}$ were homogeneously dispersed on the bottom of a 5 cm diameter glass Petri dish. After placing the sample-containing dish in the bottom of the glass box, a beaker containing a proper amount of each investigated thiol was put into the glass box, which was then closed by a glass-sealing stopper. The vapor of the thiol was then

allowed to reach the adsorption equilibrium (the vapor pressure at 20°C) within the closed glass box. During the experiment care was taken not to let the thiol-containing beaker get dry.

The content in C, N and S of the exposed Mt and Mt-Fe(III)Phen$_{sat}$ samples was analyzed as a function of time (typically 1-312 hours for SC7 and SC11, up to 30 days for the other thiols). Mt by itself does not adsorbs any thiols (see S3, Table S1), for this reason it will no longer be considered hereinafter.

The samples of Mt-Fe(III)Phen$_{sat}$ treated with the thiols for the longest time (under vapor saturation condition) are hereafter indicated as Mt-FePhen$_{sat}$-SC7, Mt-FePhen$_{sat}$-SC11, Mt-FePhen$_{sat}$-SC6OH, Mt-FePhen$_{sat}$-SC11OH, Mt-FePhen$_{sat}$-SC5COOH and Mt-FePhen$_{sat}$-SC10COOH. The elemental analyses of the samples (C, N, S) were used to measure the adsorption kinetics and the maximum amount of each thiol adsorbed by Mt-Fe(III)Phen$_{sat}$.

Thermal desorption experiments were performed heating Mt-FePhen$_{sat}$-SC7 at 110, 130, 160 or 240 °C for 10 min before performing the next adsorption/desorption cycle in order to investigate the reversibility of the thiols adsorption/desorption reaction and thus the recovery of the material. Elemental analyses were performed before and after each thermal cycle. In all cases, for times longer than 10 minutes, the amount of residual sulfur inside the thermal-treated Mt-FePhen$_{sat}$-SC7 does not change appreciably.

The above immobilization procedure was also used to investigate the interaction of SC7, SC6OH, SC11OH and SC5COOHwith Mt-Fe(III)Phen$_{semi-sat}$ at different exposure times. The samples of Mt-Fe(III)Phen$_{semi-sat}$ extensively exposed to the above thiols (due to the very different vapor pressure, the saturation time for Mt-Fe(III)Phen$_{semi-sat}$ is about 120 hrs for SC7 and SC6OH, about 28 days for SC11OH andSC5COOH) will hereafter be indicated as Mt-FePhen$_{semi-sat}$-SC7, Mt-FePhen$_{semi-sat}$-SC6OH, Mt-FePhen$_{semi-sat}$-SC11OH and Mt-FePhen$_{semi-sat}$-SC5COOH. Also for these samples, elemental analyses (C, N, S) were performed.

2.4. Analytical Methods

UV-Vis and diffuse-reflectance (DR) UV-Vis measurements were performed using a UV-Vis spectrophotometer V-570 Jasco Instrument. Measurements on Fe(III)Phen solutions were made in the range λ=220-800 nm with a bandwidth of 1 nm. For solid samples (Mt-Fe(III)Phen and thiol-exposed Mt-Fe(III)Phen samples) the spectrophotometer was equipped with an integrating sphere attachment (Jasco model ISN-470) and the measurements were made in the range λ=220-900 nm using Mt as reference. FT-IR measurements were performed using a JASCO FT/IR 4700

(resolution: 0.4cm^{-1}). The samples were disks of KBr containing Mt-Fe(III)Phen or thiol-exposed Mt-Fe(III)Phen (typically 2% w/w). The elemental analyses on the samples (C, N, S) were performed by a Carlo Erba Elemental Analyzer (Model 1106).

Thermogravimetric analyses (TGA) were made with a Seiko SSC 5200 thermal analyzer equipped with a quadrupole mass spectrometer (ESS, GeneSysQuadstar 422) which allowed analyzing the gases evolved during the thermal reactions (mass spectrometry evolved gas analysis, MS-EGA). Gas sampling by the spectrometer was via an inert, fused silicon capillary system, heated to prevent gases condensing. Gas analyses were carried out in Multiple Ion Detection mode (MID) to determine the nature of the evolved chemical species with temperature (or time). Background subtraction was used to obtain the point zero conditions before starting MID analysis.

Measurements were performed on each air-dried sample at the following experimental conditions: heating rate: 20°C/min; heating range: 25-1200°C; data measurement: every 0.5 sec; purging gas: ultrapure helium, flow rate: 100μL/min. Mass analyses were carried out in multiple ion detection mode measuring the m/z ratios 17 and 18 for H_2O, 28 and 44 for CO_2, 30 for NO and NO_2, 34 for H_2S, 46 for NO_2, and 48, 64, 66 for SO_2, 55, 56, 70, 97, 98, and 132 for SC7 (where m/z is the dimensionless ratio between the mass number and the charge of an ion); SEM and FARADAY detector at 1100V were employed with 1 sec of integration time on each measured mass. To avoid differences in relative humidity, samples were equilibrated for 15 min inside the oven using a 100 μL/min flow of ultrapure helium.

X-ray powder diffraction (XRPD) was used to detect periodicity variation along *c* in Mt-Fe(III)Phen$_{sat}$ after the exposure to thiols. XRPD patterns were recorded from (00l) oriented mounts of the air-dried samples in the temperature range 25°C≤T≤600°C (heating rate 5°C/min) using a Philips X'Pert PRO diffractometer equipped with X'Celerator detector (CuK-α radiation, 40 kV and 40 mA; 4≤ 2θ≤ 20°, quartz as calibrating standard), and HTK16 Anton Paar *in situ* heating apparatus. d_{001} diffraction patterns were collected every 20°C step of temperature increment. The position of each (001) peak has been determined at the mid-height of the reflection, using the software X-Pert High Score Plus.

Fe *K*-edge XAS spectra were collected at European Synchrotron Radiation Facility (ESRF, Grenoble, France) on the Spanish CRG Beam Line (SpLine, BM25 Branch A). The storage ring conditions were 6 GeV working in the current range 180-200 mA. A Si(111) double-crystal monochromator was used, providing an energy resolution of ~ 0.9 eV at the Fe *K*-edge, which is much less than the Fe *K* natural line width (~ 1.15 eV). For all spectra, a metallic Fe reference foil was used to provide an energy calibration for the monochromator; energy reproducibility was determined in ± 0.05 eV. Data were collected both in transmission and in fluorescence mode at

room conditions on about 10 mg of powdered samples mounted between two layers of adhesive Kapton film. The spectra were recorded over a range of 500 eV across the Fe absorption K-edge with 0.5 eV energy step in the X-ray Absorption Near-Edge Structure (XANES) region (7100-7150 eV) and 0.025 $Å^{-1}$ in the Extended X-ray Absorption Fine Structure (EXAFS) region (7150-7500 eV). Several reference compounds were measured (as detailed hereafter) to achieve a correct interpretation of samples spectra. Data reduction and analysis were performed using the Athena/Artemis interface of the IFFEFIT software.[32,33] Radial structure functions (RSF) were obtained by Fourier transforming k^3-weighted spectra in the k range 2-10$Å^{-1}$ using a Kaiser-Bessel window function ($\tau = 1$),[34,35] and compared with those of reference compound (discussion section).

RESULTS

3.1. DR UV-Vis Measurements

Mt-Fe(III)$Phen_{sat}$ after interaction with SC7or SC11shows a fast and intense chromatic effect (Figure 1). In fact, just after a few minutes of exposure the color of Mt-Fe(III)$Phen_{sat}$, initially yellow ochre (Figure 1a), turns to a red color that gets progressively more intense. After 6 hours the samples show a deep ruby red color (Figure 1b). On the contrary, the samples of Mt-Fe(III)$Phen_{sat}$ exposed to SC6OH maintain a yellow-ochre color (Figures 1c, d). The same behavior was observed when exposing Mt-Fe(III)$Phen_{sat}$ to SC11OH, SC5COOH or SC10COOH. For Mt-Fe(III)$Phen_{semi-sat}$ (Figures 1e, g), an evident and fast chromatic effect is observed after exposure to both SC7 (Figure 1f) and SC6OH (Figure1h).

DR-UV-Vis measurements performed on Mt-Fe(II)$Phen_3$, Mt-Fe(III)$Phen_{sat}$, Mt- $FePhen_{sat}$-SC7, Mt- $FePhen_{sat}$-SC6OH, yielded the spectra shown in Figure 2. The spectra of Mt-Fe(III)$Phen_{sat}$ and Mt-Fe(III)$Phen_{semi-sat}$ show a profile similar to that of the Fe(III)Phen complex in solution.[26] In particular, the band at λ=374 nm (a well-resolved shoulder is present in solution at λ=356 nm, Figures S1a and S1b) is due to the O^{2-}(bridge) $\rightarrow$ Fe(III) charge-transfer transition[36] and is typical for the ferric form of the complex. Conversely, the spectra of Mt-$FePhen_{sat}$-SC7 (Figure 2) and Mt-$FePhen_{sat}$-SC11 (see S4, Figure S3) strictly resemble that of Fe(II)$Phen_3$ complex in solution,[37] or immobilized on montmorillonite (Figure 2). In particular, a composite band with the maximum at λ=518 nm corresponds to the characteristic d $\rightarrow\pi^*$ metal-to-ligand charge transfer band of the Fe(II)$Phen_3$ complex,[37] while the band of the Fe(III) at λ=374 nm disappears. In the case of Mt-$FePhen_{sat}$-SC6OH (Figure 2), Mt-$FePhen_{sat}$-SC11OH, Mt-$FePhen_{sat}$-SC5COOH and Mt-$FePhen_{sat}$-SC10COOH (see S4, Figure S3) the spectra are quite similar to that of Mt-Fe(III)$Phen_{sat}$; only a weak band at about λ=518 nm can be observed, but much smaller than that at λ=374 nm.

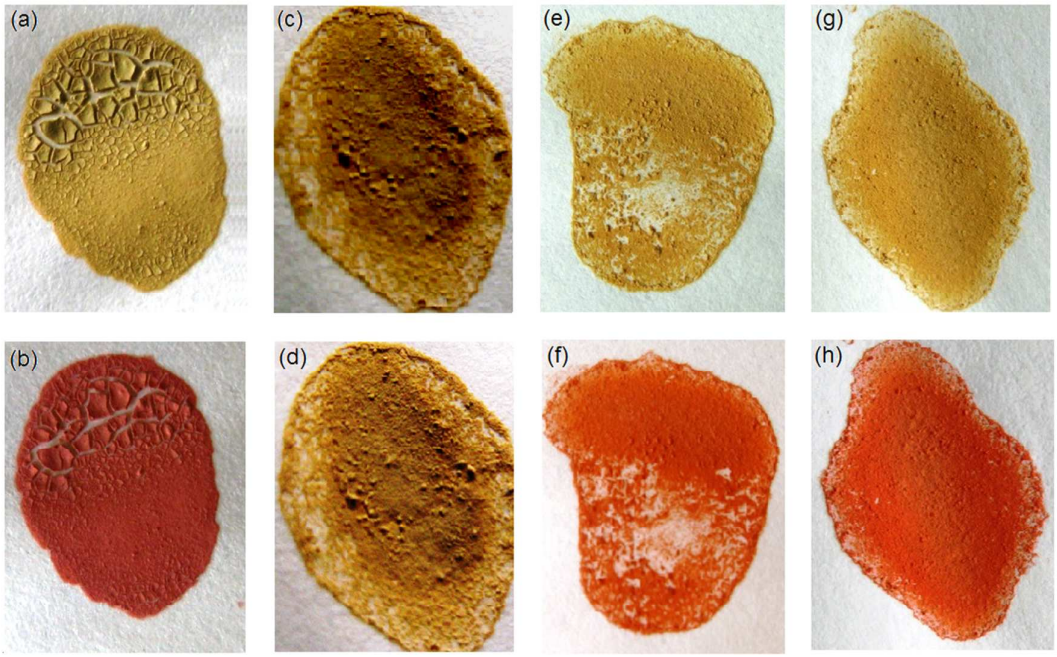

Figure 1. Mt-Fe(III)Phen$_{sat}$ before (a, c) and after 6 hours of exposure to SC7 vapor (b) and after 30 days of exposure to SC6OH vapor (d); Mt-Fe(III)Phen$_{semi-sat}$ before (e, g) and after 6 hours of exposure to SC7 vapor (f) and after 24 hours of exposure to SC6OH vapor (h).

Unlike the Mt-FePhen$_{sat}$, not only the spectrum of Mt-FePhen$_{semi-sat}$-SC7, but also that of Mt-FePhen$_{semi-sat}$-SC6OH is similar to that of Fe(II)Phen$_3$[37] and strictly resembles the spectrum of Mt-FePhen$_{sat}$-SC7 (see S5, Figure S4).

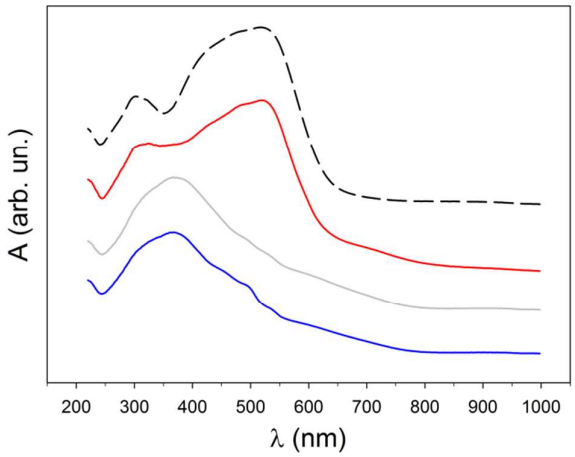

Figure 2. DR UV-Vis spectra of Mt-Fe(II)Phen$_3$ (dashed black line), Mt-FePhen$_{sat}$-SC7 (red line), Mt-Fe(III)Phen$_{sat}$ (grey line), and Mt-FePhen$_{sat}$-SC6OH (blue line). The DR UV-Vis spectrum of Mt-Fe(III)Phen$_{semi-sat}$ is similar to that of Mt-Fe(III)Phen$_{sat}$.

3.2. FT-IR measurements

The IR spectrum from 4000 to 400 cm^{-1} of Mt is shown in Figure 3. The stretching ν(OH) bands of the octahedral OH groups appear in the 3680-3550 cm^{-1} range. Two vibrations at 3630 and 3623 cm^{-1}can be observed embedded in this band. This can be due to the effect of the cation substitutions on the ν(OH) frequencies, in particular to the presence of AlOHAl and AlOHMg domains for OH groups or to a different local environment.[38] In fact, the frequency of the ν(OH) band of these groups depends also on the interactions of these bonds with the surrounding oxygen atoms of the tetrahedral shell. These frequencies are clearly lower than that of the parent mineral pyrophyllite (ν(OH) =3675 cm^{-1}). This difference can be confidently attributed to the effect of octahedral substitution of Mg^{2+} that generates an extra charge in the surrounding oxygen atoms, and to the consequently stronger hydrogen bonding or electrostatic interactions with the hydrogen atoms of OH groups. The broad band at 3540-3020 cm^{-1} can be assigned to ν(OH) modes of water molecules overlapping several bands where the frequency differences are due to the strength of the hydrogen bonding of water molecules. The band at 1644 cm^{-1} is related to the bending of the adsorbed water,[39] and the doublet at 1087 and 1041 cm^{-1} to the stretching of Si(Al)-O bonds.[40-44]

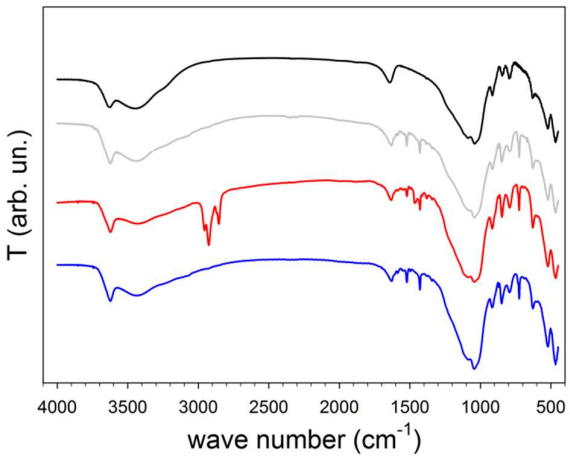

Figure 3. IR spectra of Mt (black line), Mt-Fe(III)$Phen_{sat}$ (grey line), Mt-$FePhen_{sat}$-SC7 (red line), Mt-$FePhen_{sat}$-SC6OH (blue line). The IR spectra of Mt-Fe(III)$Phen_{semi-sat}$ and Mt-$FePhen_{sat}$-SC11 strictly resemble those of Mt-Fe(III)$Phen_{sat}$ and Mt-$FePhen_{sat}$-SC7, respectively.

The structural OH-bending mode in montmorillonite absorbs between 700 and 950 cm^{-1} and shows a series of discrete peaks related to the cation composition in the octahedral sheet, namely 915 cm^{-1} (AlOHAl groups), 845 cm^{-1} (AlOHFe groups), and 796 cm^{-1} (AlOHMg groups).[41,43] The silicate features (stretching at 1087 and 1041 cm^{-1} and bending at 522 and 466 cm^{-1}) occur as doublets likely because of differences in tetrahedral site size.[42] In the IR spectrum, the immobilization of the Fe(III)Phen complex in montmorillonite (Mt-$FePhen_{sat}$ and Mt-$FePhen_{semi-sat}$) leads to the

appearance of some bands typical of Phen coordinated to the Fe (III) ion.[45-48] Other characteristic signals are not observed since they fall in correspondence of strong bands due to the Mt (Figure3). In particular, a broad shoulder is observed in the 3200-2900 cm^{-1}range that did not appear in Mt,which can be assigned to ν(CH) bands of the Phen moieties. In this complex, the area of the water bands is lower than in Mt, indicating a lower relative amount of water. The bands at 1588, 1522, 1496 and 1429 cm^{-1} are related to ring vibrations (CC and CN stretchings), while those at 871 and 722 cm^{-1} are due to out-of-plane CH bending vibrations (aromatic and heterocyclic ring, respectively). The observed bands are similar but not identical to that reported for $Fe^{3+}(Phen)_3$.[48] This fact can reasonably be attributed to the different structure of Fe(III)Phen with respect to $Fe^{3+}(Phen)_3$, but also to the adsorption and structural phenomena involving Fe(III)Phen in Mt. The bands of Mt are almost unchanged with the exception of the band at 1644 cm^{-1} that weakens considerably and shifts to 1630 cm^{-1} (Figure3). Subsequent exposure of Mt-Fe(III)$Phen_{sat}$ to SC7or SC11causes only a slight shift of the bands of the complex (1585, 1520, 1493, 1427, 872, 724 cm^{-1}) (Figure3). The limited displacement of the IR bands can be associated with the reduction of Fe(III) to Fe(II). In fact, similar differences in wave numbers were previously observed between the solid complexes $Fe^{3+}(Phen)_3$ and Fe(II)$(Phen)_3$.[48] Besides the above reported differences, the IR spectrum of Mt-Fe(III)$Phen_{sat}$ exposed to SC7 (or SC11) shows four new bands at 2953, 2926, 2871 and 2859 cm^{-1} which can be related to C-H stretching of heptanethiol (or undecanethiol) interacting with Mt-Fe(III)$Phen_{sat}$. The band at 2859 cm^{-1}can be assigned to the symmetric stretching vibration of CH_2, whereas those at 2953 cm^{-1} and 2926 cm^{-1} to the antisymmetric stretching vibration of CH_2 and CH_3 groups, respectively.[49-51] The C-S stretching vibration gives rise to a very weak absorption in the infrared spectrum,[52] and cannot be observed in our conditions. No band associated to the S-H stretching vibration (sharp and weak signal at 2550-2600 cm^{-1}) is observed.[52,53] The exposure of Mt-Fe(III)$Phen_{sat}$ to SC6OH (Figure 3), SC11OH, SC5COOH and SC10COOH (see S6, Figure S5) does not lead to any change in the IR spectrum.

The IR spectrum of Mt-Fe(III)$Phen_{semi\text{-}sat}$ exposed to SC7 (or SC6OH) shows strong signals attributable to the C-H stretching of the alkyl chain of heptanethiol (or 6-mercapto-1-hexanol) interacting with Mt-Fe(III)Phen (see S7, Figure S6).[49,50,54] In both the cases, no band due to the S-H stretching vibration is observed.[52,53]

3.3. Elemental analysis (C, N, S)

Elemental analyses (C, N, S) were performed on Mt-Fe(III)$Phen_{sat}$ before and after exposure at different times to SC7, SC11, SC6OH, SC11OH, SC5COOH and SC10COOH (Table 1, Figure 4). As already reported,[26] for Mt-Fe(III)$Phen_{sat}$ before exposure the molar ratio C/N is that expected

from the formula of Fe(III)Phen complex (C/N = 6), while the presence of S is attributable to the co-adsorption of SO_4^{2-} ions. Upon exposure to SC6OH, SC11OH, SC5COOH and SC10COOH the (C, N, S) content is unchanged, indicating the absence of any interaction between Mt-Fe(III)$Phen_{sat}$ and the –OH and –COOH terminated thiols.

Table 1. C, N, S content expressed as number of moles for 100 g of Mt for materials not-exposed and exposed to thiols (exposure up to maximum thiol adsorption). S_{thiol} and C_{thiol} stand for the moles of S and C deriving from thiol in 100 g of Mt. The associated errors (in moles/100g Mt) are for C ±0.022, for N ±0.004 and for S ±0.002. C/N, S/N, S_{thiol}/N, C_{thiol}/S_{thiol} indicate molar ratios. 100 g of Mt corresponds to 130 g of Mt-Fe(III)$Phen_{sat}$ and 112 g of Mt-Fe(III)$Phen_{semi\text{-}sat}$.

	C	N	S	C_{thiol}	S_{thiol}	C/N	S/N	S_{thiol}/N	C_{thiol}/S_{thiol}
	(moles/100g Mt)								
Mt-Fe(III)$Phen_{sat}$	1.048	0.174	0.044	–	–	6.02	0.25	–	–
Mt-Fe$Phen_{sat}$-SC7	2.911	0.176	0.310	1.863	0.266	16.54	1.76	1.51	7.01
Mt-Fe$Phen_{sat}$-SC11	3.925	0.175	0.305	2.877	0.261	22.43	1.74	1.49	11.02
Mt-Fe$Phen_{sat}$-SC6OH	1.044	0.175	0.045	nd	nd	5.97	0.26	nd	nd
Mt-Fe$Phen_{sat}$-SC11OH	1.046	0.172	0.043	nd	nd	6.08	0.25	nd	nd
Mt-Fe$Phen_{sat}$-SC5COOH	1.051	0.174	0.046	nd	nd	6.04	0.26	nd	nd
Mt-Fe$Phen_{sat}$-SC10COOH	1.049	0.175	0.045	nd	nd	5.99	0.26	nd	nd
Mt-Fe(III)$Phen_{semi\text{-}sat}$	0.529	0.088	nd	–	–	6.01	nd	–	–
Mt-Fe$Phen_{semi\text{-}sat}$-SC7	1.469	0.089	0.132	0.940	0.132	16.51	1.48	1.48	7.12
Mt-Fe$Phen_{semi\text{-}sat}$-SC6OH	1.302	0.087	0.127	0.773	0.127	14.97	1.46	1.46	6.09
Mt-Fe$Phen_{semi\text{-}sat}$-SC11OH	1.787	0.086	0.114	1.261	0.114	20.31	1.32	1.32	11.06
Mt-Fe$Phen_{semi\text{-}sat}$-SC5COOH	1.127	0.087	0.119	0.596	0.119	13.10	1.37	1.37	5.01

Nd, not determined since S or C_{thiol} and S_{thiol} are under detection limit

On the opposite, upon exposure to SC7 and SC11 the S (and C) content strongly increases with time to reach a constant value after about 13 and 20 days, respectively (Figure 4a and b). The plot of S content *vs.* time (Figure 4a and b) shows that the process takes place in two distinct steps, the latter of which is slow. The former step corresponds approximately to 2/3 of the maximum amount of the thiol that can be immobilized inside the Mt interlayer, while the latter to the remaining 1/3. For SC7 and SC11 the C/S molar ratio calculated by the increase in the C and S amount with respect to Mt-Fe(III)$Phen_{sat}$ before exposure (C_{thiol}/S_{thiol}) is that expected from the formula of a thiolate or disulfide (Table 1, formula molar ratio is C_{thiol}/S_{thiol} = 7 and 11 for SC7 and SC11, respectively, see discussion). The same behavior is observed for Mt-Fe(III)$Phen_{semi\text{-}sat}$ exposed to SC7, SC6OH, SC11OH and SC5COOH (Table 1, formula molar ratio is C_{thiol}/S_{thiol} = 7, 6, 11 and 6, respectively). In fact, in all the cases an evident increase in S and C content occurs, corresponding to the C/S molar ratio of a thiolate or disulfide species (Table 1).

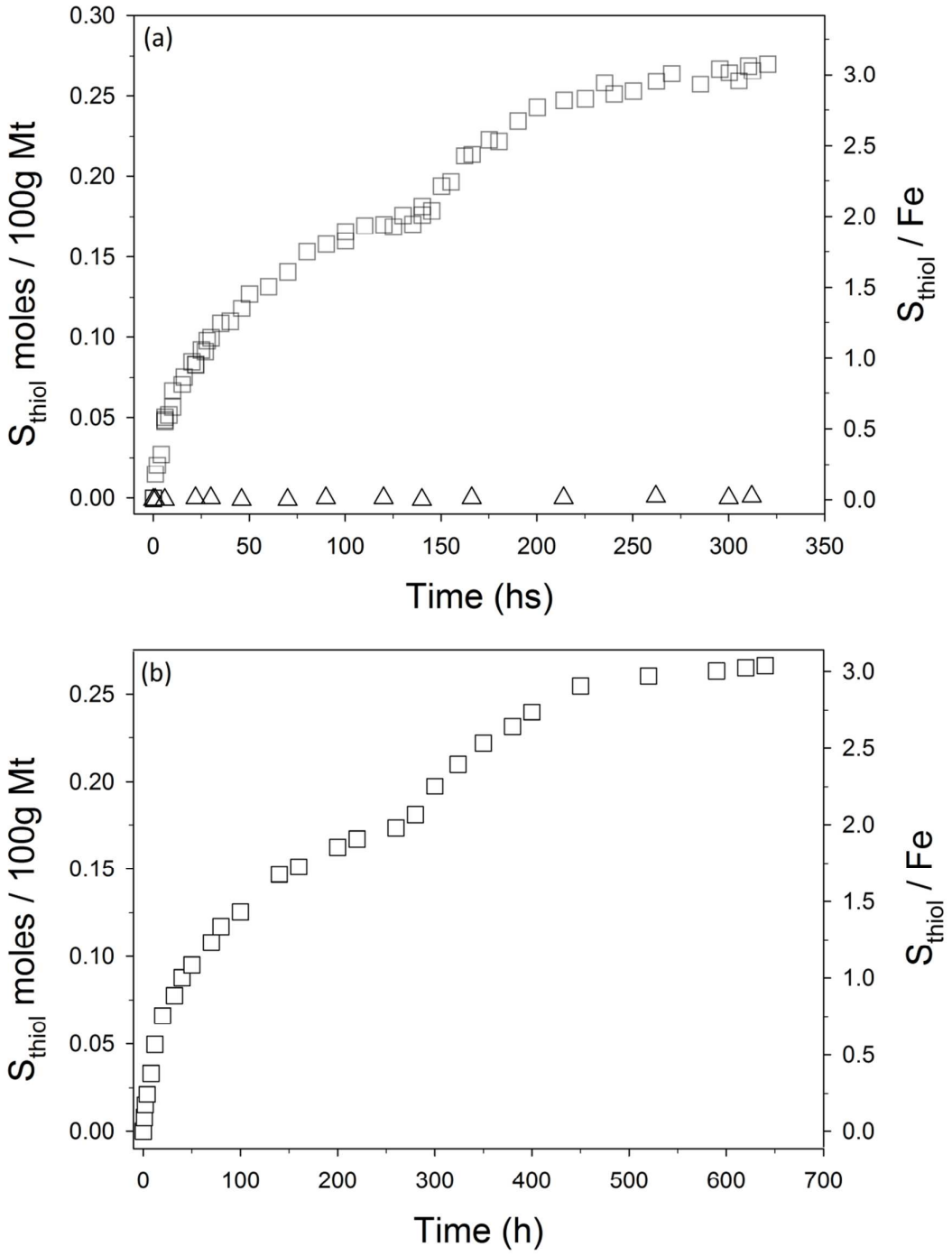

Figure 4. Plot of S moles from thiol (S_{thiol}) in 100 g of Mt (left y-axis) and S_{thiol}/Fe molar ratio (right y-axis) for Mt-Fe(III)$Phen_{sat}$ as a function of exposure time to SC7 (a, square), SC6OH (a, triangle) and SC11 (b, square). 100 g of Mt corresponds to 130 g of Mt-Fe(III)$Phen_{sat}$.

Table 2 reports the maximum S_{thiol}/Fe molar ratio for materials exposed to thiols and effective as gas trap. This S_{thiol}/Fe ratio can be confidently assumed to be 3.

Table 2. Maximum S content deriving from thiols and Fe content expressed as number of moles for 100 g of Mt, and S_{thiol}/Fe molar ratio for the not-exposed and exposed materials effective as gas trap. 100 g of Mt corresponds to 130 g of Mt-Fe(III)$Phen_{sat}$ and 112 g of Mt-Fe(III)$Phen_{semi-sat}$

	S_{thiol} (moles/100g Mt)	Fe (moles/100g Mt)	S_{thiol} / Fe
Mt-Fe(III)$Phen_{sat}$	–	0.088	–
Mt-Fe$Phen_{sat}$-SC7	0.266	0.088	3.04
Mt-Fe$Phen_{sat}$-SC11	0.261	0.088	2.99
Mt-Fe(III)$Phen_{semi-sat}$	–	0.044	–
Mt-Fe$Phen_{semi-sat}$-SC7	0.132	0.044	2.97
Mt-Fe$Phen_{semi-sat}$-SC6OH	0.127	0.044	2.86
Mt-Fe$Phen_{semi-sat}$-SC11OH	0.114	0.044	2.56
Mt-Fe$Phen_{semi-sat}$-SC5COOH	0.119	0.044	2.68

3.4. Room and temperature-controlled X-ray powder diffraction

Room temperature XRPD patterns (see S8, Figure S7) and the behavior of (d_{001}) basal reflections *vs*. temperature (see S9, Figure S8) are similar for Mt-Fe(III)$Phen_{sat}$ before and after long-lasting exposure to SC7, SC11, SC6OH, SC11OH, SC5COOH and SC10COOH, indicating that interaction with thiol does not cause meaningful variations of layer periodicity.

3.5. TGA and MS-EGA

Thermal behavior of Mt-Fe(III)$Phen_{sat}$ before exposure to thiols was previously reported.[26] After exposure to SC6OH, SC11OH, SC5COOH and SC10COOH, the thermogravimetric curves of Mt-Fe(III)$Phen_{sat}$ remain unchanged. However, the thermal behavior of Mt-Fe(III)$Phen_{sat}$ exposed to SC7 (or SC11) shows major changes (Figure 5). In the case of Mt-Fe$Phen_{sat}$-SC7, the TGA curve and its first derivative (DTGA) show: i) two well-defined thermal reactions with maxima (DTGA curve) at T=70 and 185°C associated with mass loss of 4.3 and 15.4%, respectively; ii) a poorly defined reaction at 350°C, which is better revealed in evolved gasses mass spectrometry curves (Figure6) and associated with a mass loss of 0.53%; iii) a strong composite band between 400 and 700°C due to the overlapping of three consecutive thermal reactions with maxima at 480, 550 and 620°C, altogether associated with a mass loss of 7.3%. Reactions at T>700°C, related to the thermal evolution of the decomposed complex and Mt, are not considered here because they were described previously for Mt-Fe(III)Phen.[26]

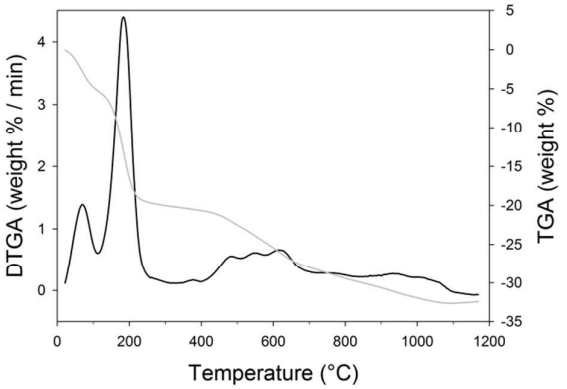

Figure 5. Thermogravimetric curves (TGA, grey line; DTGA, black line) of Mt-FePhen$_{sat}$-SC7.

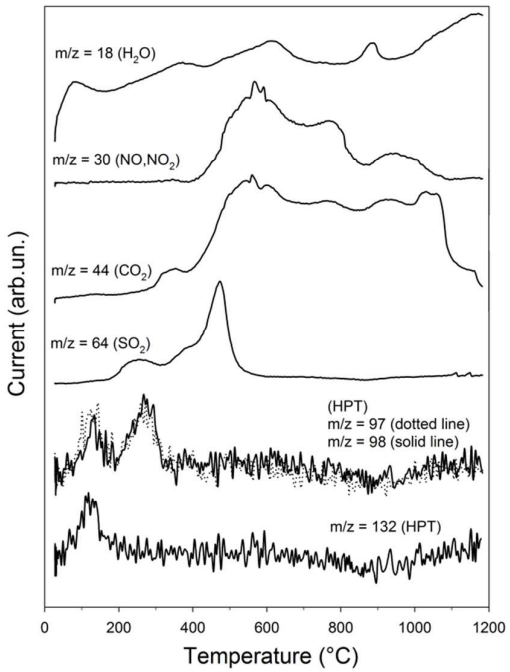

Figure 6. Mass analysis of the evolved gasses as a function of temperature for Mt-FePhen$_{sat}$-SC7 recorded at m/z = 18 (H_2O), 30 (NO and NO_2), 44 (CO_2), 64 (SO_2), 97, 98, and 132 (SC7).

MS-EGA curves (Figure 6) indicate that the reaction at 70°C is associated to the dehydration (H_2O release, m/z=18). The thermal desorption of the immobilized thiol or its derivatives occurs in the thermal range 95-260°C (peak in DTGA at 185°C). Parent thiol release is associated with the peak observed at 135°C in the MS-EGA curve (SC7 release, m/z =132, 98 and 97), whereas SO_2 (m/z = 64) and alkyl fragments (m/z= 97 and 98) evolve in the T range 195-260°C. Although the two processes are not resolved in TGA and DTGA curves (Figure5), they can be easily observed in MS-EGA curves (Figure 6, m/z=132, 98 and 97).

In Mt-Fe(III)Phen$_{sat}$, both before and after exposure to thiol, CO_2, SO_2 and NO_x emissions occur between 305 and 390°C and between 400 and 700°C (Figures 5, 6). The signal between 305 and 390°C can be tentatively assigned to the thermal decomposition of the complex located at the Mt surface,[26]accordingly to the changes observed in the IR spectrum at T = 350°C (the bands in the region 1250-1500 cm^{-1}, typical of the aromatic ligand, completely disappear, see S10, Figure S9). The composite signal at higher temperature (400-700°C) can be associated with the thermal decomposition of the iron complex in Mt interlayer.[26]

3.6. Thermal desorption and reversibility of the interaction of Mt-Fe(III)Phen with thiols

Freshly prepared Mt-FePhen$_{sat}$-SC7 and Mt-FePhen$_{sat}$-SC11were heated at 110, 130, 160 and 240°C to optimize the conditions for material regeneration, in particular the lowest temperature at which a complete quick thiol removal is still possible and the highest temperature at which thiol removal occurs leaving unchanged the Mt-Fe(III)Phen$_{sat}$ adsorption properties towards thiols. The changes in the sulfur content at 110, 130, 160 and 240 °C *vs.* time are reported in Figure 7. At 110, 130 and 160 °C the sulfur content associated to the thiol decreases to one third of the initial content, with a rate depending on the treating temperature. The complete desorption of the immobilized sulfur-derivatives (thiol and disulfide)can be obtained only at 240°C (the residual sulfur content, due to sulfate ions, can be removed only at T > 400°C.[26] The thermal treatment at T≤240°C is fully reversible for at least 20 cycles (Figure8), *i.e.* the hybrid material can thermally release and, afterwards, uptake thiol again in the same amount and with a similar time course (Figure 8). On the opposite, the thermal treatment at T=350°C drives to chemical and structural changes that no longer allow further uptakes of the sulfur derivatives (Figure 8).

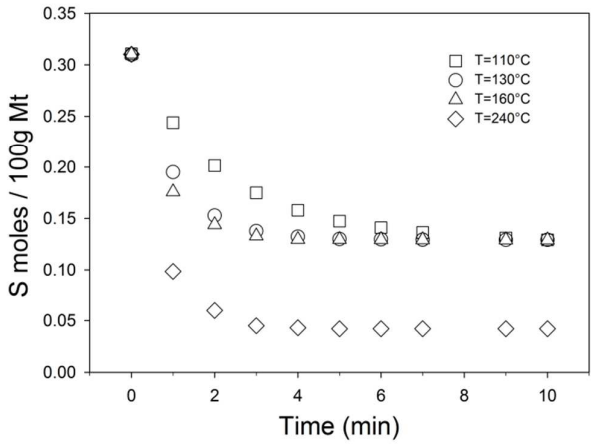

Figure 7. Plot of total S moles (S) in 100 g of Mt *vs.* time for Mt-FePhen$_{sat}$-SC7 treated at different temperatures: T = 110 (square), 130 (circle), 160 (triangle), and 240°C (diamond). 100 g of Mt corresponds to 130 g of Mt-Fe(III)Phen$_{sat}$.

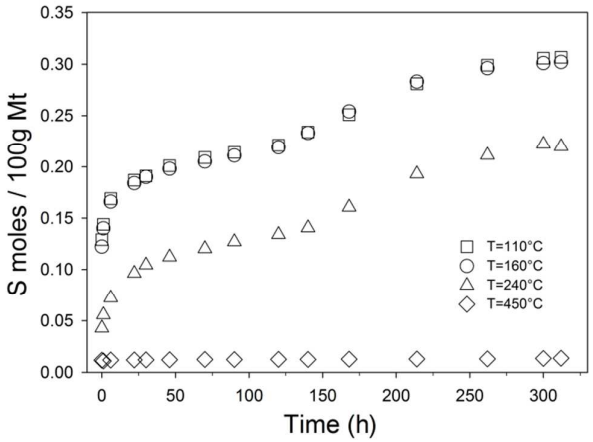

Figure 8. Plot of total S moles (S) in 100 g of Mt for Mt-Fe(III)Phen$_{sat}$ as a function of exposure time to SC7 after 20 desorption/adsorption cycles; desorption processes were made at T = 110 (square), 160 (circle), 240 (triangle) and 450°C (diamond). The adsorption results irreversible when SC7 is desorbed at T > 350°C (e.g. 450°C, diamond).100 g of Mt corresponds to 130 g of Mt-Fe(III)Phen$_{sat}$.

Accordingly, thermal treatments at T ≤240°C do not change the IR spectrum of Mt-Fe(III)Phen$_{sat}$, except for the signals related to water. On the contrary, the thermal treatment of the samples at T=350°C leads to radical changes or disappearance of the phenanthroline bands (Figure 9).

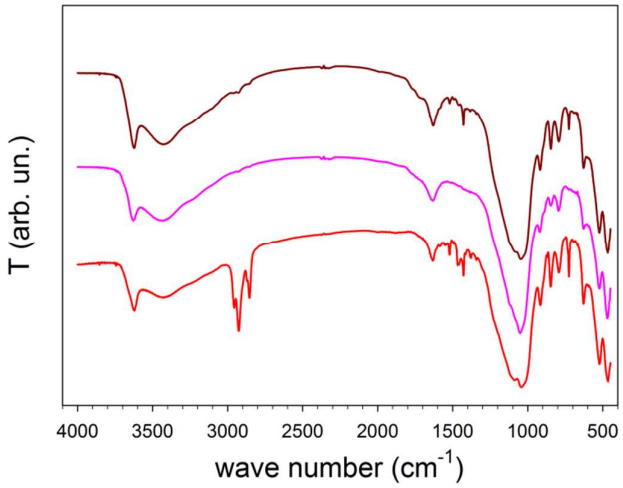

Figure 9. IR spectra of Mt-FePhen$_{sat}$-SC7 before (red line) and after heating for 1 hour at 240 (pink line) and 350°C (brown line).

3.7 X-ray Absorption Spectroscopy

XAS data at Fe-*K* edge allow measurement of Fe^{3+} to Fe^{2+} reduction when Mt-Fe(III)Phen is exposed to thiol and, therefore, it is informative on its effectiveness as redox-switch-based gas trap. Pre-edges peaks observed in *K* edge XANES spectra of transition metal are related to 1s → 3d quadrupolar electronic transition and/or 1s → 4p dipolar electronic transitions. The pre-edge position shifts to higher energy as the oxidation state increases, and is used to determine the oxidation state of Fe.

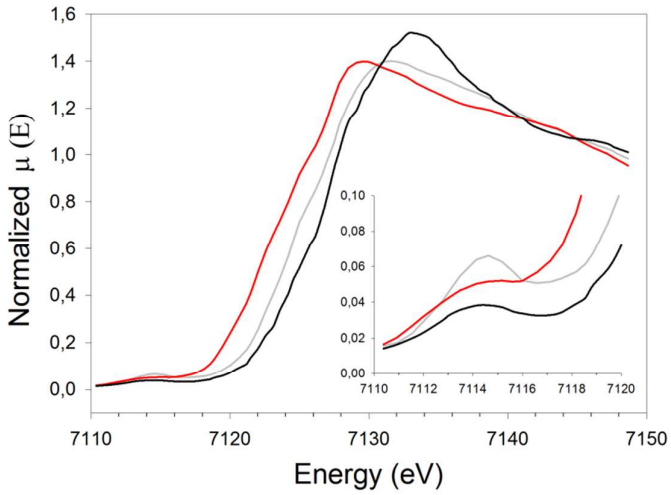

Figure 10. XANES spectra of Mt (black line), Mt-Fe(III)Phen$_{sat}$ (grey line) and Mt-FePhen$_{sat}$-SC7 (red line), a magnification of the pre-edge region is also provided.

Figure10 compares XAS spectra of Mt, Mt-Fe(III)Phen$_{sat}$, and Mt-FePhen$_{sat}$-SC7. All spectra in the 7100-7200eV energy region contain a pre-edge (~7114-7115eV), a shoulder (~7123-7126eV), and a crest (~7129-7133eV), arising from transitions to final states that include significant 3d, 4s and 4p components, respectively, and post-edge structure associated with multiple scattering and transitions to delocalized and continuum levels. Features commonly used to quantify $Fe^{3+}/\Sigma Fe$ are the weak 1s→3d pre-edge, the 1s→4s shoulder, and the 1s→4p crest in the energy ranges indicatedabove.[55,56] The comparison among spectra of Figure 10 points out several differences:

i) Pre-edge shape and position. Mt sample hosts Fe^{3+} in tetrahedral position, thus giving a pre-edge. Both treatments with the complex and exposure to SC7 should not modify iron in such position; therefore the variations in the pre-edge shape (see magnification in Figure10) could be related to the interference of signal coming from iron bond to phenanthroline.

ii) Energy position of the shoulders and the crests. Both shoulders and crests shift to lower energy after exposure to SC7, indicating a change in the iron oxidation state.

DISCUSSION

Affinity towards thiols. Mt-Fe(III)Phen shows a high affinity towards thiols, which is intriguing. It is even higher than that obtained with gold nanoparticles supported on metal oxides.[27] In fact, Mt-Fe(III)Phen$_{semi-sat}$ can immobilize large amounts of thiol (up to 3:1 S/Fe molar ratio), independently of the nature of the ending tail. On the contrary, Mt-Fe(III)Phen$_{sat}$ strongly and quickly interacts only with thiols bearing a hydrophobic (methyl) tail(heptanethiol saturated Mt-Fe(III)Phen$_{sat}$ contains up to 5.2 % in weight of S, *i.e.* 21.3% w/w in thiol), but does not adsorb at all those terminating with hydrophilic groups (–OH or –COOH). The reason of this "hydrophobically driven" interaction of Mt-Fe(III)Phen$_{sat}$ can reasonably be attributed to the strong structuring effect of Fe(III)Phen inside the Mt interlayer.[26] This iron complex can be described as a box in which the two phenanthroline ligands are nearly parallel to each other and is characterized by an extensive aromatic moiety.[57] The structuring of the interlayer, therefore, probably involves the formation of a sort of "strongly hydrophobic channels" through which only hydrophobic molecules can diffuse. Accordingly, the observed decrease of the water content associated with the adsorption of Fe(III)Phen inside the Mt interlayer nicely agrees with an increase in hydrophobicity of the interlayer.[26]Consequently, thiols bearing hydrophilic groups cannot diffuse inside the channels. In the case of Mt-Fe(III)Phen$_{semi-sat}$ the amount of adsorbed iron complex is lower and occurs simply through a cation exchange process without structuring effects, thereby allowing the thiols to freely diffuse inside the interlayer.

The possibility to increase the hydrophobicity and the affinity towards organic molecules of the interlayer of some clay minerals like montmorillonite is well known.[58-60] In our case, however, Mt-Fe(III)Phen$_{sat}$ results extremely selective towards thiols and specifically towards the end group of the alkyl chain. The length of the chain does not play any apparent role in the interaction process. These results suggest that the architecture of the interlayer pillared by a host complex can be used to render it highly sensitive to specific structural details of the guest molecule.

Thiol immobilization mechanism and kinetics. The interaction mechanism of thiol with Fe(III)Phen and its immobilization inside the interlayer are complex processes which include several steps. In fact, spectroscopic data indicate that, upon the exposure to the thiol, Fe^{3+} in the complex undergoes reduction to Fe^{2+} and this reaction is likely associated to the oxidation of thiol to disulfide in a redox pathway. The resulting Fe^{2+} complex (probably Fe(II)Phen) rapidly binds a first thiolate ion and, eventually, a second one at a lower rate. The IR spectra lack the signal related to S-H stretching (2550-2600 cm^{-1}, Figure3) confirming the absence of (physi-)adsorption of thiol molecules. The mechanism of thiol immobilization occurring in montmorillonite can be, therefore, summarized as follows (for sake of clarity, water molecules are omitted):

$$[PhenFe(III)\text{-}O\text{-}Fe(III)Phen]^{4+} + 2\ CH_3\text{-}RSH \rightarrow 2\ [PhenFe(II)]^{2+} + CH_3\text{-}RS\text{-}SR\text{-}CH_3 + H_2O \quad \text{fast} \quad (1)$$

$$2\ [PhenFe(II)]^{2+} + 2\ CH_3\text{-}RSH \rightarrow 2\ [PhenFe(II)SR\text{-}CH_3]^{+} + 2\ H^{+} \quad \text{fast} \quad (2)$$

$$2\ [PhenFe(II)\text{-}SR\text{-}CH_3]^{+} + 2\ CH_3\text{-}RSH \rightarrow 2\ [PhenFe(II)(SR\text{-}CH_3)_2] + 2\ H^{+} \quad \text{slow} \quad (3)$$

corresponding to the overall reaction:

$$[PhenFe(III)\text{-}O\text{-}Fe(III)Phen]^{4+} + 6\ CH_3\text{-}RSH \rightarrow CH_3\text{-}RS\text{-}SR\text{-}CH_3 + 2\ [PhenFe(II)(SR\text{-}CH_3)_2] + H_2O + 4\ H^{+}$$

Four protons are produced to compensate the decrease of positive charge of the iron in the dinuclear complex which switches from +4 to 0 due to reduction and immobilization of two thiolates. These protons are adsorbed on the Mt lattice (Mt-Fe(III)Phen$_{semi\text{-}sat}$) or are both adsorbed on the Mt lattice and neutralize sulfate ions inside the interlayer (Mt-Fe(III)Phen$_{sat}$). The pH decrease due to thiol immobilization was confirmed by pH measurements performed on 4M NaCl solutions exchanged with Mt-Fe(III)Phen$_{sat}$, Mt-Fe(III)Phen$_{semi\text{-}sat}$, Mt-FePhen$_{semi\text{-}sat}$-SC7, and Mt-FePhen$_{sat}$-SC7 (namely, a rough evaluation of the pH of these materials, for details see S11); the pH of the solutions exchanged with both Mt-Fe(III)Phen$_{sat}$ and Mt-Fe(III)Phen$_{semi\text{-}sat}$ was 6.42, while the pH

of the solutions exchanged with Mt-FePhen$_{semi-sat}$-SC7 and Mt-FePhen$_{sat}$-SC7 were found to be 3.91 and 3.07, respectively.

The proposed mechanism is in good agreement also with the time dependence of the uptake of the thiol by Mt-FePhen$_{sat}$. In fact, Figure 4 shows two different steps. The former is fast with a limit immobilization value corresponding to a 1:2 iron/thiol molar ratio (the Fe(III) amount in Mt-FePhen$_{sat}$ is 0.0878 moles/100g Mt),[26] which could correspond to the oxidation of the thiol to disulfide and the subsequent uptake of one thiolate ion by Fe(II)Phen. The latter, slower, step corresponds to an uptake of a second thiolate ion to yield a total limit value of 1:3 iron/thiol molar ratio (Table 2, Figure 4a and b). The presence of the thiolate species is shown by the IR spectra. Unfortunately, the bands typical of the disulfide (w, 705-570 cm^{-1} for C-S stretching and w, 620-600 cm^{-1} for S-S stretching) fall on the strong bands of montmorillonite and therefore cannot be observed. The presence of two types of sulfur derivatives, however, is indirectly confirmed by the thermal analysis of Mt-FePhen$_{sat}$-SC7 (Figure 5). In fact, S-derivatives are observed in the gas produced by the thermal treatment in two well defined temperature ranges: between 85 and 195 °C the intact thiol is produced, but between 195 and 260 °C the S-containing species observed in MS-EGA is SO_2along with fragments corresponding to the alkyl group of the thiol. This result can be interpreted as follows. Between 85 and 195 °C the thiolate ion linked to Fe(II) is released as thiol, but not the disulfide, since it is not volatile. Between 195 and 260 °C the disulfide is (partially) oxidized yielding SO_2 and the corresponding alkyl fragments. The behavior of Mt-Fe(III)Phen$_{semi-sat}$ against both hydrophilic and hydrophobic thiols parallels that of Mt-Fe(III)Phen$_{sat}$ interacting with hydrophobic thiols, therefore the same mechanism involving three steps reasonably occurs also in this case. According with mechanism (1)-(3), a reaction forming [PhenFe(II)(S(CH$_2$)$_6$-CH$_3$)$_2$(H$_2$O)$_2$] and CH$_3$-(CH$_2$)$_6$S-S-(CH$_2$)$_6$-CH$_3$ from [PhenFe(III)-O-Fe(III)Phen]$^{4+}$ and CH$_3$-(CH$_2$)$_6$SH has been obtained in ethanol (see S12, Table S2 and Figure S10).

The kinetics of saturation of Mt-Fe(III)Phen$_{sat}$ with SC7 in the first adsorption step is fast. In particular, about one third of the saturation amount is immobilized in only 22 hours (Figure 4). The fast kinetics and efficiency of the process can be nicely confirmed analyzing the time needed to remove heptanethiol by a closed box. In particular, we have investigated the removal of heptanethiol with time for 10, 25, 50 mg of Mt-Fe(III)Phen$_{sat}$ in a thiol-saturated box of 4 dm^3 containing 1 mg of liquid heptanethiol. Figure 11 shows the corresponding plots of adsorbed heptanethiol *vs.* time; using 50 mg of Mt-Fe(III)Phen$_{sat}$ the thiol is completely removed within 2 hours.

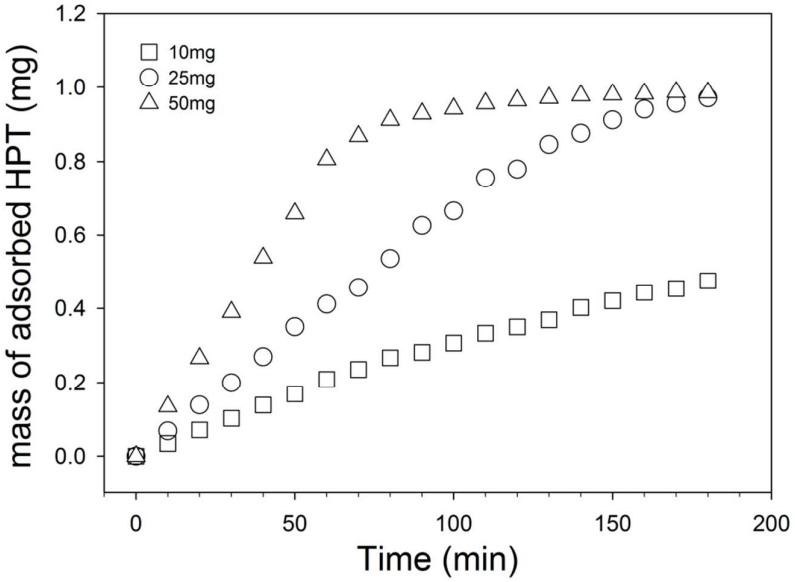

Figure 11. Plots of adsorbed SC7mass *vs.* time for 10 (square), 25 (circle), 50 mg (triangle) of Mt-Fe(III)Phen$_{sat}$ in a SC7-saturated box of 4 dm^3 containing 1 mg of liquid SC7.

XANES spectra of samples in which $Fe^{3+}/\Sigma Fe$ varies are likely to exhibit systematic differences in the energy and intensity of pre-edge, edge, and post-edge features, any of which could be used for empirical quantification. To confirm the oxidation state the comparison with spectra of well know compounds must be considered.

Figure 12 shows the XANES spectra of Mt-Fe(III)Phen$_{sat}$ and, as reference compounds, the pure grade reagents $Fe_2(SO_4)_3{\cdot}nH_2O$, $[Fe(o\text{-phen})_3]SO_4$ (ferroin), and $FeSO_4$, the minerals hematite (Fe_2O_3) and magnetite ($FeOFe_2O_3$), and the powder of the Fe(III)Phen crystal we have synthesized with formula $[(OH_2)_3(Phen)FeOFe(Phen)(OH_2)_3]^{+4}(SO_4)_2$.

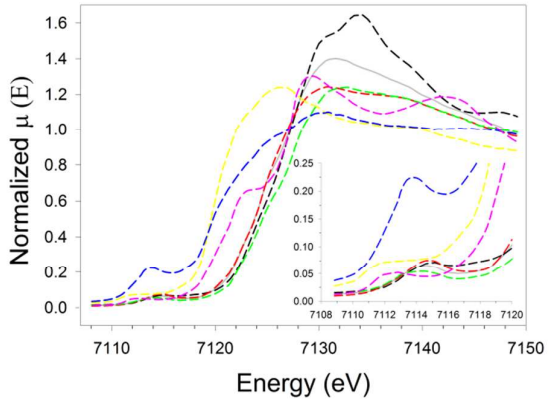

Figure 12. XANES spectra of Mt-Fe(III)Phen$_{sat}$ (grey line) and of the reference compounds $Fe_2(SO_4)_3{\cdot}nH_2O$ (dashed green line), $[Fe(o\text{-phen})_3]SO_4$ (dashed pink line), $FeSO_4$ (dashed yellow line), hematite (dashed black line), magnetite (dashed blue line), and the powder of the synthesized Fe(III)Phen crystal (dashed red line). A magnification of the pre-edge region is also provided.

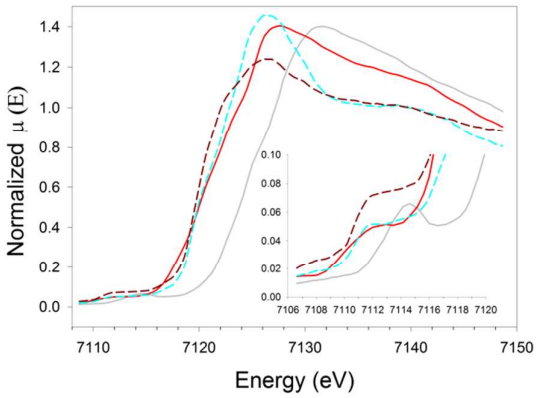

Figure 13. XANES spectra of Mt-Fe(III)Phen$_{sat}$ (grey line), Mt-FePhen$_{sat}$-SC7 (red line) and of the reference compounds $FeSO_4$ (dashed brown line) and $Fe(NH_4)_2(SO_4)_2{\cdot}6H_2O$ (dashed cyan line). A magnification of the pre-edge region is also provided.

Comparison of the spectra shows a marked similarity in shape and position of the XANES regions of Mt-Fe(III)Phen$_{sat}$ and Fe(III)Phen crystal. A further confirmation of the similarity between the structure of Mt-Fe(III)Phen$_{sat}$ and that of synthesized Fe(III)Phen crystal is provided by the atomic radial function and back transformed Fourier function reported in Figure S11 (see S13), suggesting a very similar local structure around iron in both samples, at least for distance and occupation of first and second neighbors. The energy values of absorption edges and crests due to 1s→4p transitions of Mt-Fe(III)Phen$_{sat}$ parallel those of reference compounds $Fe_2(SO_4)_3 \cdot nH_2O$, and hematite (Fe_2O_3) where iron is always trivalent. On the contrary, differences arise when comparing spectra of Mt-Fe(III)Phen$_{sat}$ with that of the reference compound magnetite (where both Fe^{2+} and Fe^{3+} are present) and, in particular, with that of $FeSO_4$ (where divalent iron only is present). The edge position as well as the line shape of the pre-edge peak of Mt-Fe(III)Phen$_{sat}$ are a clear evidence that the sample contains only trivalent Fe ions.

Analogously, similarities and differences can be observed in Figure 13, which shows the spectra of Mt-Fe(III)Phen$_{sat}$, Mt-FePhen$_{sat}$-SC7 and those of the pure grade reagents $FeSO_4$ and $Fe(NH_4)_2(SO_4)_2 \cdot 6H_2O$ as reference compounds. The pre-edge shift to lower energy confirms the reduction of Fe^{3+} to Fe^{2+} by the thiol adsorption.

Minor discrepancies between the spectra of Mt-FePhen$_{sat}$-SC7 and reference compounds containing only divalent iron should be attributed to small amount of trivalent iron in the tetrahedral and octahedral sheet of montmorillonite that is unaffected both by the intercalation of the complex and by exposure to heptanethiol.

The peculiar affinity of Fe(III)Phen towards hydrophobic thiols results both in the relevant amount of thiol that can be immobilized (Mt-FePhen$_{sat}$-SC7 contains up to 5.2 % in weight of S from thiol, *i.e.*, 21.3 %in weight of SC7) and in the fast kinetics of interaction observed for the first step of adsorption. In fact, although the analysis of the kinetics was not attempted, we confidently assume that the fast kinetics and efficiency of the process is nicely confirmed analyzing the time requested to completely remove thiol in a closed box, as above reported.

Desorption mechanism and reversibility. From 110 to 160°C (Figure 7) desorption of the thiol from Mt-FePhen$_{sat}$-SC7 is fast, but does not go to completion, involving only for 2/3 of the total amount. The reaction which restores the starting heptanethiol is:

$$[PhenFe(II)(SR\text{-}CH_3)_2] + 2\ H^+ \leftrightarrows\ [PhenFe(II)]^{+2} + 2\ CH_3\text{-}R\text{-}SH \quad (4)$$

At 240 °C the thiol is fully desorbed and the adsorption/desorption process is reversible according to reaction (4). Up to 160°C desorption involves only 2/3 of the total amount of immobilized thiol (corresponding to the thiolate ligand), afterwards in the temperature range 200-300°C also the disulfide is desorbed (Figures 5, 6). The temperature-dependent cycle corresponding to reaction (4) can be repeated several time (we tested 20 cycles at 240°C) without remarkable changes in the kinetics of immobilization. The adsorption/desorption process becomes progressively irreversible when the release of NO, NO_2, and CO_2 begins, *i.e*. when the complex undergoes pyrolysis. The IR bands related to phenanthroline do not change from room temperature to 300°C, suggesting that thermal treatment does not damage the molecular structure of the intercalated Fe(III)Phen which is effective in thiol immobilization. Afterwards, at temperatures higher than 350°C, when the iron complex loses its ability to immobilize thiol molecules, also the IR spectra show changes in the bands related to the aromatic ring according to the thermal decomposition of iron complex.

CONCLUSIONS

The hybrid material Mt-Fe(III)Phen, obtained by an easy, fast and reproducible intercalation process of the μ-oxo Fe(III)-phenanthroline complex into montmorillonite, is imparted with the relevant property of entrapping huge amounts of thiols in the gas phase. This is due to the formation of a strong covalent bond between the sulfur atom of the thiol and the ferrous ion of the complex, providing a stable immobilization. This process represents a step ahead with respect to all other processes which rely on thiol physi-adsorption: in our case the thiol immobilization massively occurs even at room temperature and pressure and this is much more advantageous with respect to other desulfurization processes which require more severe conditions and energy supply. In addition, thiol catching is fully reversible: the entrapping material can be thermally regenerated and brought back to its full immobilizing capacity quickly and in mild conditions. This further contributes to cut the operating costs of this process.

The efficiency of Mt-Fe(III)Phen as a gas trap is tuned by the complex saturation level which modulates the hydrophobicity of the material. The semi-saturated Mt-Fe(III)Phen is effective in the immobilization of both hydrophobic and hydrophilic thiols; conversely, the saturated material shows a strong binding selectivity based on the hydrophobicity of the thiol molecule: only thiols bearing no hydrophilic groups enter the interlayer and are trapped therein.

The reason for this selectivity has to be sought in the high structuring of the interlayer in saturated Mt-Fe(III)Phen which probably results in the formation of a network of strongly hydrophobic channels lined by the aromatic components of the Fe(III)Phen aggregates.

Since the mechanism that controls gas immobilization involves a redox reaction and the formation of an iron-sulfur bond, we are convinced that it is possible to expand the opportunities offered by this approach employing other metal-chelate complexes having redox properties and affinity to sulfur atom, and extending the research to the study of the immobilization of H_2S.

Supporting Information

The on-line Supporting Information (PDF) contains: UV-Vis spectra of Fe(III)Phen at pH 2.5 and 5.1 as a function of time (S1); UV-Vis spectra of solutions exchanged with Mt-Fe(III)$Phen_{semi-sat}$ and Mt-Fe(III)$Phen_{sat}$ (S2); elemental analysis of Mt and Mt exposed to thiols (S3); DR UV-Vis and IR spectra of Mt-Fe(III)$Phen_{sat}$ and Mt-Fe(III)$Phen_{semi-sat}$ after exposure to different thiols (S4-S7); XRPD measurements (full patterns and d_{001} values up to 560°C) of Mt-Fe(III)$Phen_{sat}$ before and after exposure to SC7 (S8, S9); IR spectrum of Mt-Fe$Phen_{sat}$-SC7 heated at 350°C (S10); pH of exchanged solutions before and after thiol immobilization (S11); Separation and identification of the products obtained by the reaction between $[PhenFe(III)\text{-}O\text{-}Fe(III)Phen]^{4+}$ and $CH_3\text{-}(CH_2)_6SH$ in ethanol: $CH_3\text{-}(CH_2)_6\text{-}S\text{-}S\text{-}(CH_2)_6\text{-}CH_3$ and $[PhenFe(II)(S\text{-}(CH_2)_6\text{-}CH_3)_2(H_2O)_2]$ (S12); XAS spectra of Mt-Fe(III)$Phen_{sat}$ and the synthesized Fe(III)Phen crystal (S13).

Acknowledgments

Our research enjoys the support of the European Synchrotron Radiation Facility (ESRF) – experiment CH-4514, October 2015 at the Spanish beam line. An appreciated support was also provided by Centro Interdipartimentale Grandi Strumenti (CIGS) of Università di Modena e Reggio Emilia and by its staff.

REFERENCES

(1) Kadijani, J. A.; Narimani, E. Simulation of Hydro Desulfurization Unit for Natural Gas Condensate with High Sulfur Content. *Appl. Petrochem. Res.* **2016**, *6*, 25−34.

(2) Pavlova, A.; Ivanova, P.; Dimova, T. Sulfur Compounds in Petroleum Hydrocarbon Streams. *Petroleum & Coal* **2012**, *54*, 9−13.

(3) Bineesh, K. V.; Kim, D.-K.; Kim, D.-W.; Cho, H.-J.; Park, D.-W. Selective Catalytic Oxidation of H_2S to Elemental Sulfur over V_2O_5/Zr-Pillared montmorillonite Clay. *Energy Environ. Sci*. **2010**, *3*, 302−310.

(4) Castellini, E.; Bortolotti, C. A.; di Rocco, G.; Bernini, F.; Ranieri, A. Enhancing Biocatalysis: The Case of Unfolded Cytochrome c Immobilized on Kaolinite. *ChemCatChem* **2013**, *5*, 1765−1768.

(5) Gupta, S. S.; Bhattacharyya, K. G. Adsorption of Heavy Metals on Kaolinite and Montmorillonite: a Review. *Phys. Chem. Chem. Phys.* **2012**, *14*, 6698−6723.

(6) Kumar, B. S.; Dhakshinamoorthy, A.; Pitchumani, K. K10 Montmorillonite Clays as Environmentally Benign Catalysts for Organic Reactions. *Catal. Sci. Technol.* **2014**, *4*, 2378−2396.

(7) Morales-Serna, J. A.; Frontana-Uribe, B. A.; Olguín, R.; Gómez-Vidales, V.; Lomas-Romero, L.; Garcia-Ríos, E.; Gaviño, R.; Cárdenas, J. Reaction Control in Heterogeneous Catalysis Using Montmorillonite: Switching Between Acid-Catalysed and Red-Ox Processes. *RSC Adv.* **2016**, *6*, 42613−42617.

(8) Ranieri, A.; Bernini, F.; Bortolotti, C. A.; Castellini, E. The Met80Ala Point Mutation Enhances the Peroxidase Activity of Immobilized Cytochrome c. *Catal. Sci. & Technol.* **2012**, ***2***, 2206−2210.

(9) Ruiz-Hitzky, E.; Aranda, P.; Darder, M.; Rytwo, G. Hybrid Materials Based on Clays for Environmental and Biomedical Applications. *J. Mater. Chem.* **2010**, ***20***, 9306−9321.

(10) Zhu, R.; Chen, Q.; Zhou, Q.; Xi, Y.; Zhu, J.; He, H. Adsorbents Based on Montmorillonite for Contaminant Removal from Water: A Review. *Appl. Clay Sci.* **2016**, *123*, 239−258.

(11) Bineesh, K. V.; Kim, D.-K.; Kim, M.-IL.; Selvaraj, M.; Park, D.-W. Design, Synthesis and Characterization of Vanadia-Doped Iron-Oxide Pillared Montmorillonite Clay for the Selective Catalytic Oxidation of H_2S. *Dalton Trans.* **2011**, *40*, 3938−3945.

(12) De Paolo, D. J.; Cole, D. R. In *Geochemistry of Geologic CO_2 Sequestration*; De Paolo, D. J.; Cole, D. R.; Navrotsky, A.; Bourg, I.C., Eds.; Mineralogical Society of America - Geochemical Society: Chantilly, Virginia, 2013; Chapter 1, pp 1−14.

(13) Giesting, P.; Guggenheim, S.; van Groos, A. F. K.; Busch, A. Interaction of Carbon Dioxide with Na-Exchanged Montmorillonite at Pressures to 640 Bars: Implications for CO_2 Sequestration. *Int. J. Greenhouse Gas Control* **2012**, *8*, 73−81.

(14) Giesting, P.; Guggenheim, S.; van Groos, A. F. K.; Busch, A. X-Ray Diffraction Study of K- and Ca-Exchanged Montmorillonites in CO_2 Atmospheres. *Environ. Sci. & Tech.* **2012**, *46*, 5623−5630.

(15) Hemmen, H.; Rolseth, E. G.; Fonseca, D. M.; Hansen, E. L.; Fossum, J. O.; Plivelic, T. S. X-ray Studies of Carbon Dioxide Intercalation in Na-Fluorohectorite Clay at Near-Ambient Conditions. *Langmuir* **2012**, *28*, 1678−1682.

(16) Kadoura, A.; Nair, A. K. N.; Sun, S. Adsorption of Carbon Dioxide, Methane, and their Mixture by Montmorillonite in the Presence of Water. *Micropor. Mesopor. Mat.* **2016**, *225*, 331−341.

(17) Loring, J. S.; Schaef, H. T.; Turcu, R. V. F.; Thompson, C. J.; Miller, Q. R. S.; Martin, P. F.; Hu, J.; Hoyt, D. W.; Qafoku, O.; Ilton, E. S.; Felmy, A. R.; Rosso, K. M. In Situ Molecular Spectroscopic Evidence for CO2 Intercalation into Montmorillonite in Supercritical Carbon Dioxide. *Langmuir* **2012**, *28*, 7125−7128.

(18) Michels, L.; Fossum, J. O.; Rozynek, Z.; Hemmen, H.; Rustenberg, K.; Sobas, P. A.; Kalantzopoulos, G. N.; Knudsen, K. D.; Janek, M.; Plivelic, T. S.; da Silva, G. J. Intercalation and Retention of Carbon Dioxide in a Smectite Clay promoted by Interlayer Cations. *Sci. Rep.* **2015**, *5*, Article number: 8775, 1-9.

(19) Nguyen-Thanh, D.; Bandosz, T. J. Effect of Transition-Metal Cations on the Adsorption of H_2S in Modified Pillared Clays. *J. Phys. Chem. B* **2003**, *107*, 5812−5817.

(20) Nguyen-Thanh, D.; Block, K.; Bandosz, T. J. Adsorption of hydrogen Sulfide on Montmorillonites Modified with Iron. *Chemosphere* **2005**, *59*, 343−353.

(21) Rao, Q.; Xiang, Y.; Leng, Y. Molecular Simulations on the Structure and Dynamics of Water-Methane Fluids between Na-Montmorillonite Clay Surfaces at Elevated Temperature and Pressure. *J. Phys. Chem. C* **2013**, *117*, 14061−14069.

(22) Achmann, S.; Hagen, G.; Hammerle, M.; Malkowsky, I.; Kiener, C.; Moos, R. Sulfur Removal from Low-Sulfur Gasoline and Diesel Fuel by Metal-Organic Frameworks. *Chem. Eng. Technol.* **2010**, *33*, 275−280.

(23) Blanco-Brieva, G.; Campos-Martin, J. M.; Al-Zahrani, S. M.; Fierro, J. L. G. Effectiveness of Metal-Organic Frameworks for Removal of Refractory Organo-Sulfur Compound Present in Liquid Fuels. *Fuel* **2011**, *90*, 190−197.

(24) Chen, G.; Tan, S.; Koros, W. J.; Jones, C. W. Metal Organic Frameworks for Selective Adsorption of t-Butyl Mercaptan from Natural Gas. *Energy Fuels* **2015**, *29*, 3312−3321.

(25) Chen, G.; Koros, W. J.; Jones, C. W. Hybrid Polymer/UiO-66 (Zr) and Polymer/NaY Fiber Sorbents for Mercaptan Removal from Natural Gas. *ACS Appl. Mater. Interfaces* **2016**, *8*, 9700−9709.

(26) Bernini, F.; Castellini, E.; Malferrari, D.; Borsari, M.; Brigatti, M. F. Stepwise Structuring of the Adsorbed Layer Modulates the Physico-Chemical Properties of Hybrid Materials from Phyllosilicates Interacting with the μ-oxo Fe^{+3}-Phenanthroline Complex. *Micropor. Mesopor. Mat.* **2015**, *211*, 19−29.

(27) Sui, R.; Lesage, K. L.; Carefoot, S. K.; Furstenhaupt, T.; Rose, C. J.; Marriott, R. A., Selective Adsorption of Thiols Using Gold Nanoparticles Supported on Metal Oxides. *Langmuir* **2016**, *32*, 9197–9205.

(28) Keshavarzi, N.; Rad, F. M.; Mace, A.; Ansari, F.; Akhtar, F.; Nilsson, U.; Berglundand, L.; Bergstrom, L. Nanocellulose–Zeolite Composite Films for Odor Elimination. *ACS Appl. Mater. Interfaces*, **2015**, *7*, 14254−14262.

(29) Weber, G.; Benoit, F.; Bellat, J.-P.; Paulin, C.; Mougin, P.; Thomas, M. Selective Adsorption of Ethyl Mercaptan on NaX Zeolite. *Microporous and Mesoporous Mater.* **2008**, *109*, 184–192.

(30) The Clay Minerals Society Database, http://www.clays.org/Sourceclays.html, accessed on December 6, 2016.

(31) Castellini, E.; Berthold, C.; Malferrari, D.; Bernini, F. Sodium Hexametaphosphate Interaction with 2:1 Clay Minerals Illite and Montmorillonite. *Appl. Clay Sci.* **2013**, *83–84*, 162–170.

(32) Newville, M. IFEFFIT: Interactive XAFS Analysis and FEFF Fitting. *J. Synchrotron Radiat.* **2001**, *8*, 322−324.

(33) Raveland, B.; Newville, M. J. Athena, Artemis, Hephaestus: Data Analysis for X-Ray Absorption Spectroscopy Using IFEFFIT. *Synchrotron Radiat.* **2005**, *12*, 537−541.

(34) Ankudinov, A. L.; Ravel, B.; Rehr, J. J.; Conradson, S. D. Real Space Multiple-Scattering Calculation and Interpretation of X-Ray Absorption Near-Edge Structure. *Phys. Rev. B* **1998**, *58*, 7565−7576.

(35) Rehr, J. J.; Deleon, J. M.; Zabinsky, S. I.; Albers, R.C. Theoretical X-ray Absorption Fine Structure Standards. *JACS* **1991**, *113*, 5135−5140.

(36) Plowman, J. E.; Loehr, T. M.; Schauer, C. K.; Anderson, O. P. Crystal and Molecular Structure of the (μ-Oxo)Bis[Aquobis(Phenanthroline)Iron(III)] Complex, a Raman Spectroscopic Model for the Binuclear Iron Site in Hemerythrin and Ribonucleotide Reductase. *Inorg. Chem.* **1984**, *23*, 3553−3559.

(37) McWhinnie, W.R.; Miller, J.D. In *Advances in Inorganic Chemistry and Radiochemistry*; Hemeléus, H.J.; Sharpe, A.G. Eds.; Academic Press: New York, 1970.

(38) Ortega-Castro, J.; Hernández-Haro, N.; Muñoz-Santiburcio, D.; Hernández-Laguna, A.; Sainz-Díaz, C. I. Crystal Structure and Hydroxyl Group Vibrational Frequencies of Phyllosilicates by DFT Methods. *J. Mol. Struc. (THEOCHEM)* **2009**, *912*, 82−87.

(39) Che, C.; Glotch, T. D.; Bish, D. L.; Michalski, J. R.; Xu, W. Spectroscopic Study of the Dehydration and/or Dihydroxylation of Phyllosilicate and Zeolite Minerals. *J. Geophys. Res.* **2011**, *116*, E05007.

(40) Bishop, J. L.; Pieters, C. M.; Edwards, J. O. Infrared Spectroscopic Analyses on the Nature of Water in Montmorillonite *Clay. Clay Miner.* **1994**, *42***,** 702−716.

(41) Bishop, J. L.; Madejová, J.; Komadel, P.; Fröschl, H. The Influence of Structural Fe, Al and Mg on the Infrared OH Bands in Spectra of DioctahedralSmectites. *Clay Miner.* **2002**, *37*, 607−616.

(42) Bishop, J. L.; Murad, E. Characterization of Minerals and Biogeochemical Markers on Mars: a Raman and IR Spectroscopic Study of Montmorillonite. *J. Raman Spectrosc.* **2004**, *35*, 480−486.

(43) Madejová, J.; Bujdák, J.; Janek, M.; Komadel, P. Comparative FT-IR Study of Structural Modifications During Acid Treatment of DioctahedralSmectites and Hectorite. *Spectrochim. Acta A* **1998**, *54*,1397−1406.

(44) Madejová, J.FTIR Techniques in Clay Mineral Studies.*Vib. Spectrosc.* **2003**, *31*, 1−10.

(45) Gerasimova, T. P.; Katsyuba, S. A. Bipyridine and Phenanthroline IR-Spectral Bands as Indicators of Metal Spin State in Hexacoordinated Complexes of Fe(II), Ni(II) and Co(II). *Dalton Trans.* **2013**, *42*, 1787−1797.

(46) König, E.; Madeja, K. Infra-red Spectra at the $^5T_2$ – $^1A_1$ cross-over in iron (II) complexes.*Spectrochim. Acta* **1967**, *23*, 45−54.

(47) Reiher, M.; Brehmand, G.; Schneider, S. Assignment of Vibrational Spectra of 1,10-Phenanthroline by Comparison with Frequencies and Raman Intensities from Density Functional Calculations. *J. Phys. Chem. A* **2004**, *108*, 734−742.

(48) Schilt, A. A.; Tayor, R. C. Infra-red Spectra of 1 : 10-Phenanthroline Metal Complexes in the Rock Salt Region Below 2000 cm^{-1}. *J. Inorg. Nucl. Chem.* **1959**, *9*,211−221.

(49) Bertilsson, L.; Liedberg, B. Infrared Study of Thiol Monolayer Assemblies on Gold: Preparation, Characterization, and Functionalization of Mixed Monolayers. *Langmuir* **1993**, *9*, 141−149.

(50) Himmelhaus, M.; Eisert, F.; Buck, M.; Grunze, M. Self-Assembly of *n*-Alkanethiol Monolayers. A Study by IR−Visible Sum Frequency Spectroscopy (SFG). *J. Phys. Chem. B* **2000**, *104*, 576−584.

(51) Uehara, T. M.; de Aguiar, H. B.; Bergamaski, K.; Miranda, P. B. Adsorption of Alkylthiol Self-Assembled Monolayers on Gold and the Effect of Substrate Roughness: A Comparative Study Using Scanning Tunneling Microscopy, Cyclic Voltammetry, Second-Harmonic Generation, and Sum-Frequency Generation. *J. Phys. Chem. C* **2014**, *118*, 20374−20382.

(52) Coates, J. In *Encyclopedia of Analytical Chemistry*; Meyers, R.A., Ed.; John Wiley & Sons Ltd: Chichester, 2000, pp 10815−10837.

(53) Yablonskii, O. P.; Rodionova, N. M.; Lapuka, L. F. An Infrared Spectroscopic Study of Hydrogen Bonding in Thiols. *J. Appl. Spectrosc.* **1973**, *19*, 1303−1305.

(54) Tielens, F.; Costa, D.; Humblot, V.; Pradier, C.-M. Characterization of ω-Functionalized Undecanethiol Mixed Self-Assembled Monolayers on Au(111): A Combined Polarization Modulation Infrared Reflection-Absorption Spectroscopy/X-ray Photoelectron Spectroscopy/Periodic Density Functional Theory Study. *J. Phys. Chem. C* **2008**, *112*, 182−190.

(55) Berry, A. J.; Danyushevsky, L. V.; O'Neill, HStC.; Newville, M.; Sutton, S. R. The Oxidation State of Iron in Komatiitic Melt Inclusions Indicates Hot Archaean Mantle. *Nature* **2008**, *455*, 960−963.

(56) Tombolini, F.; Brigatti, M. F.; Marcelli, A.; Cibin, G.; Mottana, A.; Giuli, G. Local and Average Fe Distribution in Trioctahedral Micas: Analysis of Fe K-Edge XANES Spectra in the Phlogopite-Annite and Phlogopite-Tetraferriphlogopite Joins on the Basis of Single-Crystal XRD Refinements. *Eur. J. Mineral.* **2002**, *14*, 1075−1085.

(57) Healy, P. C.; Patrick, J. M.; White, A. H. Crystal Structure of μ-Oxo-bis-fac-[triaqua-1,10-Phenanthrolineiron(III)] Tetrakis(nitrate) Monohydrate. *Aust. J. Chem.* **1984**, *37*, 1405−1410.

(58) Lee, S. M. and Tiwari, D. Organo and Inorgano-Organo-Modified Clays in the Remediation of Aqueous Solutions: An Overview. *Appl. Clay Sci.* **2012**, *59-60*, 84−102.

(59) van Oss, C. J.; Giese, R. F. The Hydrophilicity and Hydrophobicity of Clay Minerals. *Clay. Clay Miner.* **1995**, *43*, 474−477.

(60) de Paiva, L. B.; Morales, A. R.; Valenzuela Díaz, F. R. Organoclays: Properties, Preparation and Applications. *Appl. Clay Sci.* **2008**, *42*, 8−24.

Table of Contents/Abstract Graphic